Understanding the role of mass transport kinetic on reversible and irreversible capacity losses in lithium sulfur batteries

Journal of Energy Storage 168 (2026) 122660

Contents lists available at ScienceDirect

Journal of Energy Storage

journal homepage: www.elsevier.com/locate/est

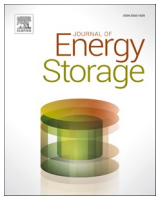

Research Papers

Understanding the role of mass transport kinetic on reversible and irreversible capacity losses in lithium sulfur batteries

Tommaso Filippo Lupatelli [a,*], Massimo Santarelli [a], Silvia Bodoardo [b], Daniele Versaci [b]

[a] Synergy of Thermo-chemical and Electro-chemical Power Systems (STEPS), Department of Energy, Polytechnic of Turin, corso Duca degli Abruzzi 24, 10129, Turin, Italy

[b] Electrochemistry Group, Department of Applied Science and Technology, Polytechnic of Turin, corso Duca degli Abruzzi 24, 10129, Turin, Italy

ARTICLE INFO

Keywords:
Lithium sulfur
Multiscale modeling
Irreversible and reversible capacity losses
Shuttling
Cell design

ABSTRACT

Lithium sulfur batteries (Li—S) have reached a growing interest in the research and industrial sector as reliable candidate as post-Lithium-ion batteries, due to their high theoretical specific capacity and the low cost involving the supply chain. However, their practical implementation faces several challenges due to the intrinsic complexity of a system based on conversion chemistry and the presence of dissolved active species in the electrolyte. In this work it is reported the effect of limited mass transport on reversible and irreversible capacity loss in a 1D framework. A parametric analysis was performed on different cases related to lithium diffusivity within the electrolyte, focusing not only on short- and long-term capacity but also on its effects on the potential curves and on the structural evolution of the cathode. The model has been proven able to simulate the experimentally observed consequences of shuttling, highlighting the necessity to look towards a common ground for the future optimization of Li—S batteries.

1. Introduction

Rechargeable batteries are a key technology enabling energy storage for many applications, since they can: accelerate the shift towards sustainable and smart mobility; help supply clean, affordable, and secure energy and mobilize industry for a cleaner, circular economy including full life cycle assessment (LCA). On the other side, it must be considered that LIBs are gradually approaching their theoretical energy-density limit, which is determined by intrinsic intercalation chemistry, after decades of improvements on all battery components and packing engineering. The interest is now focused on high-capacity electrodes to pursue higher energy density, as lithium anodes, sulfur, and oxygen cathodes. As sulfur is a very low cost and highly available resource, Lithium–sulfur batteries (Li—S) highlight a promising next generation energy storage system because of the large theoretical gravimetric energy density of 2600[$Whkg^{-1}$] and volumetric energy density of 2800 [WhL^{-1}] [1]. Li—S provides a multielectron redox couple at the sulfur cathode and therefore guarantees the large increase in discharge capacity in comparison to intercalation systems. The high theoretical specific capacity of Li—S batteries arises from the multistep redox conversion reaction ($S_8 + 16\ Li^+ + 16\ e^- \rightarrow 8\ Li_2S_{(s)}$) that involves a series of "solid–liquid–solid" reactions: the long and complicated reduction reactions can be divided into two main steps with the respective voltage plateaus being located at 2.3 and 2.1 V versus Li^+/Li. The first step is related to the conversion of solid S_8 to liquid polysulfide intermediates (S_8^{2-}, S_6^{2-}, and S_4^{2-}) with a theoretical capacity of 419 [$mAhg^{-1}$] according to the four electrons transferred per S_8. The other step is the formation of final insulating products $Li_2S_{(s)}$, which contributes to a theoretical capacity of 1256[$mAhg^{-1}$] according to the 12 electrons transferred per S_8 [2,3]. The sluggish redox kinetics of multiple polysulfide solid/liquid conversion reactions present several dynamic challenges, and the unwanted shuttling of lithium polysulfides (LiPSs) intermediates makes it extremely difficult to achieve both high sulfur utilization and high cyclability and rate ability. It has been well established that the conversion from solid $S_{8(s)}$ to liquid polysulfide intermediates (Li_2S_x, $4 \leq x \leq 8$) is a relatively easy process because of the low activation energy. Nevertheless, the subsequent liquid to solid $Li_2S_{2(s)}/Li_2S_{(s)}$ reactions requires a much higher activation energy, and the solid-to-solid conversion of $Li_2S_{2(s)}$ to $Li_2S_{(s)}$ is the rate-determining step in sulfur chemistry [4,5].

However, the most critical issue of Li—S system is related to LiPSs dissolution. On one hand, dissolution of LiPSs is beneficial to achieve full active-material utilization because new bulk sulfur can be continuously exposed to the electrolyte and participate in the reaction. On the other

* Corresponding author.
E-mail address: tommaso.lupatelli@polito.it (T.F. Lupatelli).

https://doi.org/10.1016/j.est.2026.122660
Received 19 January 2026; Received in revised form 21 April 2026; Accepted 10 May 2026
Available online 16 May 2026

hand, the dissolved long chain polysulfides can diffuse out of the cathode and migrate towards the anode, where they directly react with metallic lithium creating nonconductive and insoluble $Li_2S_{(s)}$ precipitate on its surface. This process is known as "polysulfides shuttle effect", which results in both anode corrosion and irreversible loss of active material, with consequent low-capacity retention and low Coulombic efficiency. Moreover, during cell resting, sulfur reacts directly with lithium ions in the electrolyte producing soluble lithium polysulfides with consequent self-discharge of the cell. The relatively short cycle life, compared with conventional Li-ion technology, has its source in the use of a lithium metal-based negative electrode, especially in combination with highly reactive polysulfides.

Modeling can be a valuable tool for the future development of Li—S batteries, allowing for rapid and straightforward investigations without the time-consuming and costly experimental setup and control procedures. As mentioned above, LiS battery cells' chemistry is quite different from the typical Li-ion cells' chemistry, therefore, a new modeling approach must be followed. Y. V. Mikhaylik and J. R. Akridge published in 2004 one of the first article on mathematical models for charging-discharging of Li—S batteries [6]; in their zero dimensional (0D) model the reduction of sulfur was divided into two steps, corresponding respectively for the high and low voltage plateau, and employing Nernst-Planck equation. Their model precisely predicts the impact of shuttle on the cell. Indeed, as the current applied decreases or the shuttle phenomena become more relevant, the sulfur is not fully oxidized and therefore the cell will never be fully charged. However, the discharge profiles obtained did not accurately replicate the typical Li—S evolution, indicating that a single reaction for the high plateau is insufficient to fully represent the cell's electrochemistry. Moreover, the model overlooks the activation overpotential and the electrolyte's conductivity dependence on the ionic species' concentration, both of which influence the cell's voltage. Marinescu et al. [7] proposed an alternative 0D model for the assessment of the shuttle effect in their study, still based on a two-reaction scheme with an irreversible loss of active material expressed by a dimensionless loss rate. In Marinescu's model, the sulfur loss is not solely determined by the shuttle rate or dissolved sulfur, but also by the sulfur that has already been shuttled, effectively accounting for the aging effect on the cell's performance, thus accounting for an active sulfur loss, without specifying a particular location. A successive step on continuum modeling of shuttling was made by Kamyab et al. in 2020 [8], which introduces a chemical approach to describe shuttling as source for irreversible losses. The model was developed in a one-dimensional (1D) framework, therefore allowing us to implement also mass transport limitations in the study. Kamyab model was able to provide a persistent capacity decay and an overall wider understanding of polysulfides shuttling. Nevertheless, the model was limited to a few cycles number and it oversimplifies the description of shuttling. At first, the reaction was treated as bulk reaction, which is instead limited at the anode/electrolyte interphase; furthermore, the reduction of polysulfides at the anode does not account the gradual formation of lower order polysulfides but assumes immediate losses, therefore neglecting potential consequences on the concentration unbalance of the dissolved species.

Another benchmark for Li—S modeling was made by Kumaresan et al. [9] by developing the first 1D model. The model considers four different precipitated polysulfide species ($n = 2, 4, 6, 8$) and relies upon a five-step reaction scheme for sulfur reduction. These elements function as sinks and sources to describe the spatiotemporal variations in ionic species concentrations. The model successfully replicates the voltage profiles of Li—S batteries, capturing the key features. However, as Ghaznavi and Chen [10] have reported, it is not suitable for simulating the charging portion of the batteries due to the low saturation concentration of lithium polysulfide, even though it incorporates reversible terms. Zhang et al. [11] proved by coupling modeling and experimental activity that the 1D model developed by Kumaresan et al. underestimate the effect of limited diffusion kinetics as source of reversible losses. The model qualitatively aligns with experimental results; indeed, it can explain the decline in low-plateau capacity at high discharge rates. The slower diffusion of the polysulfides, coupled with the effect of Li^+ diffusivity on the electrolyte potential, generates a significant driving force that pushes them away from the cathode, leading to accumulation inside the separator.

In this study, it is presented a 1D model developed using COMSOL Multiphysics to understand the role of limited mass transport kinetics as source of both reversible and irreversible losses. The model simulates four different scenarios of Li^+ diffusivity to investigate its role on the polysulfides behavior and how it affects the performance on both short and long terms performances. Shuttling was described as a chemical irreversible reaction consisting of a series of reduction steps until a permanent deposition of lithium polysulfides at the anode/separator interface occurs. The adopted approach guarantees a more accurate description of the shuttling phenomenon, achieving good agreement with experimental observations reported in the literature. Moreover, it represents one of the few models reported to date that can simulate an extensive number of cycles under different operating conditions, thereby allowing a direct comparison between experimental and modeling results and providing a robust setup for future improvements in the field of Lithium Sulfur batteries.

2. Model development

The model is based on the porous electrode theory. The electrode is treated as a continuum domain where the ionic and electric transport processes occur in a porous framework, depending on the discharge/charge state. The electrochemical activity of the dissolved species is described using Butler-Volmer equation, meanwhile the transport process is controlled by Nerst-Plank equations. The mass and charge balance equation were solved in a 1D time-dependent domain, consisting of a porous cathode and separator, meanwhile the Li-metal anode is treated as a single point boundary, able to guarantee an endless amount of Li^+ [8,10–12] The used framework allows to simulate the evolution of each dissolved species within the computational domain and their distribution in a given time point. It was opted for an ideal dissolution description of the electrolyte, therefore the electric conductivity of the electrolyte is not negatively impacted by the Li^+ concentration, differently as it was discussed and proved by Zhang et al. [13]. The assumption of ideal electrolyte behavior therefore represents a simplification compared to more specific studies reported in the literature [14,15], where, depending on the ether type of solvent and sulfur to electrolyte ratio, significant variations during the single cycle can be observed. However, this assumption is motivated by the purpose of providing a general framework that is not restricted to a specific solvent system. Furthermore, incorporating modifications to the mass transport equations to account for the evolution of ionic conductivity would increase the computational cost without guaranteeing numerical stability over long simulation cycles. Indeed, as reported in the literature, studies focusing on long-term cycling commonly adopt a simplified description of the electrolyte, as do investigations specifically addressing mass transport limitations [6–8,10,11]. For the model development, only the shuttling of polysulfides has been considered as source for all the irreversible capacity losses. Shuttling was limited only during the charging phase, as during this step, the progressive buildup of high-order polysulfides within the electrolyte generates a concentration gradient that drives their diffusion from the cathode towards the anode. Upon reaching the lithium metal surface, these species are reduced due to the low electrochemical potential of lithium. Therefore, in agreement with previous studies, both experimental and modeling, reported in the literature [7,8,16–18], it was decided to limit shuttling at the charging step. Nevertheless, the model set up is still suitable to study shuttling on both charge and discharge. The reduction of dissolved polysulfides due to shuttling is confined at the anode/separator interphase and it is followed by an irreversible precipitation of $Li_2S_{(s)}$. It was implemented a

pure chemical description [7,8,17], where the reduction rate is dependent on a fixed constant k_s, so called shuttle constant, and the concentration of each polysulfide species at the interface with the Li-metal anode. The model set up was limited to 50 galvanostatic cycles at a fixed current intensity of 0.05C, without any rest between each cycle. Nevertheless, the model can be extended to a larger number of cycles, but in this study, it was limited at 50 cycles to minimize computational cost. An implicit solver was employed, using a backward differentiation formula, BDF, method for time integration. The resulting nonlinear system was solved via an automatically controlled Newton-Raphson scheme, with a minimum admissible damping factor of 10^{-8}.

2.1. Electrochemical/chemical frameworks

During discharge, the solid sulfur is gradually dissolved inside the electrolyte into $S_{8(l)}$ to be then electrochemically reduced following a cascade towards lower order polysulfides, therefore the reference initial concentration of $S_{8(l)}$ is controlled by the solubility limit reported in Table 3. Several reaction schemes can be used to describe the electrochemical conversion of sulfur, accounting for both accuracy and simplicity; at first it was assumed that the solid $S_{8(s)}$ volume fraction does not contribute to any electrochemical reaction, meanwhile the $S_{8(l)}$ dissolved inside the electrolyte is reduced according to the following scheme [8,9]:

$$\frac{1}{2}S_{8(l)} \leftrightarrow \frac{1}{2}S_8^{2-} \tag{1}$$

$$\frac{3}{2}S_8^{2-} \leftrightarrow 2S_6^{2-} \tag{2}$$

$$S_6^{2-} \leftrightarrow \frac{3}{2}S_4^{2-} \tag{3}$$

$$\frac{1}{2}S_4^{2-} \leftrightarrow S_2^{2-} \tag{4}$$

$$\frac{1}{2}S_2^{2-} \leftrightarrow S^{2-} \tag{5}$$

Two reaction approaches are widely used for its simplicity and less input parameters needed. However, a five reduction description was followed to guarantee a microscale description of the sulfur electrochemical activity allows to going deeper in the conversion chemistry that characterized lithium sulfur battery [2]. During discharge at the anode side, Li metal is oxidized according to eq. 6:

$$Li \leftrightarrow Li^+ + e^- \tag{6}$$

Lithium sulfur performances are dependent not only on the electrochemical activity of the dissolved polysulfides, but also on non-faradaic reactions. Starting from $S_{8(s)}$ dissolution, during discharge the concentration of $S_{8(l)}$ is governed by its electrochemical reduction at the carbon-electrolyte interphase, and from the gradual dissolution of solid sulfur:

$$S_{8(s)} \leftrightarrow S_{8(l)} \tag{7}$$

Theoretically, it's needed to account for the solubility limit of each dissolved polysulfides, as their precipitation leads to the deposition of an electric insulating solid phase on the cathode surface. However, in most studies, both experimental and modeling [7,13,19–21], only $Li_2S_{(s)}$ is considered as the predominant precipitated products in system using ether based solvent, which formation follows the equation below:

$$2Li^+ + S^{2-} \leftrightarrow Li_2S_{(s)} \tag{8}$$

2.2. Governing equations

The material balance for each single dissolved species inside the computational domain is controlled by the transport process inside the separator and the porous cathode. Meanwhile electrochemical and non-faradaic reactions act as sink/source terms. The separator domain is referred to with the subscript $m = sep$ meanwhile the cathode with the subscript $m = cat$. The material balance is therefore summarized as follows:

$$\frac{d(\varepsilon_m C_i)}{dt} = -\nabla \bullet N_i + r_i + R_i \tag{9}$$

where R_i derives from non-faradaic reaction, r_i represents the contribution given by electrochemical activity meanwhile:

$$r_i = a\sum \frac{s_{i,j} i_j}{n_j F} \tag{10}$$

ε_m is the porosity fraction inside the domain m, meanwhile C_i stands for the concentration of each dependent variable inside the electrolyte. The flux of each dissolved species, in agreement with the dilute solution theory, is dependent on the corrective diffusive coefficient, $D_{i,m,eff}$, the charge number of each species, z_i, and the liquid phase potential φ_l:

$$N_{i,m} = -D_{i,m,eff}\frac{dC_i}{dx} - \frac{z_i D_{i,m,eff}}{RT} F C_i \frac{d\varphi_l}{dx} \tag{11}$$

The effective diffusion coefficient $D_{i,m,eff}$ of the species i is expressed as function of the porosity of the domain m, following the Bruggeman expression:

$$D_{i,m,eff} = D_{i,m,0} * \varepsilon_m^b \tag{12}$$

Although the experimental Bruggeman coefficient b is extrapolated assuming diffusion in an isotropic spheric domain, which does not fit the actual porous structure of the sulfur-carbon cathode [11]. The transport properties and the reference concentration for each dissolved species have been taken from literature [11] and reported in Table 1

2.3. Kinetics and equilibrium potential

Butler-Volmer equation is used to define the current density for the individual electrochemical reaction j at the solid/liquid interface:

$$i_j = i_{0,ref} * \left\{ \prod_i \left(\frac{C_i}{C_i^{ref}} \right)^{p_{i,j}} \exp\left(\frac{\alpha_{a,j} F}{RT} n_j \right) - \prod_i \left(\frac{C_i}{C_i^{ref}} \right)^{q_{i,j}} \exp\left(\frac{-\alpha_{c,j} F}{RT} n_j \right) \right\} \tag{13}$$

The overpotential for each electrochemical reaction is calculated as follows:

$$n_j = \varphi_s - \varphi_l - U_{j,ref} \tag{14}$$

Concerning the open circuit voltage, the Nernst voltage equations are implemented, accounting for the concentration of each dissolved species C_i involved in the electrochemical reaction j with respect to the reference concentration, corrected with the factor 1000 to move from moles per liter to moles per unit:

$$U_{j,ref} = U_j^0 - \frac{RT}{n_j F}\sum_i s_{i,j} ln\left[\frac{c_{i,ref}}{1000}\right] \tag{15}$$

Table 1
Transport properties and Reference concentrations [11].

Specie (i)	z_i	$D_{i,0}\,[m^2 s^{-1}]$	$C_{i,ref}\,[mol\ m^{-3}]$
Li^+	1	0.88e-11	1001
A^{-1}	-1	3.5e-12	1000
$S_{8(l)}$	0	0.88e-11	19
S_8^{2-}	−2	3.5e-12	0.18
S_6^{2-}	−2	3.5e-12	0.32
S_4^{2-}	−2	1.75e-12	0.02
S_2^{2-}	−2	0.88e-12	5.23e-6
S^{2-}	−2	0.88e-12	8.27e-8

According to equation, the total liquid-phase current density i_l, is dependent on both liquid phase potential and concentrations:

$$i_l = F\sum_I z_i N_i \tag{16}$$

Meanwhile, the solid-phase charge transfer, i_s, inside the porous cathode domain is defined by the Ohm's Law, with the major assumption of a constant electric conductivity through cycling:

$$i_s = -\sigma\nabla\varphi_s \tag{17}$$

The following equation is used to guarantee the exchange of current inside the liquid phase only through electrochemical reaction:

$$\nabla i_l = a\sum_j i_j \tag{18}$$

where a stands for the specific surface area of the cathode, corrected as function of the empirical parameters ξ and for the available interface between the electrolyte and the conductive network, as it is assumed that both the precipitated $S_{8(s)}$ and $Li_2S_{(s)}$ are not electrochemical conductive:

$$a = a_o\left(\frac{\varepsilon_{cat}}{\varepsilon_{cat,o}}\right)^{\xi} \tag{19}$$

Lastly, the charge conservation inside the porous electrode, which means that the charge leaving a phase must be compensated, as follows (Table 2):

$$\nabla \bullet i_s = \nabla \bullet i_l \tag{20}$$

2.4. Kinetic for non-faradaic reaction

As mentioned above, during discharge $S_{8(s)}$ is gradually dissolved into $S_{8(l)}$, and soluble polysulfides inside the electrolyte. The kinetic description of such reaction should be able to account the reversible nature of the process and so describe both dissolution and precipitation. Therefore it was decided to implement the approach employed by Kamyab et al. in their model [8]:

$$R_{S_{8(s)}} = k_{S_{8(s)}}\varepsilon_{S_{8(s)}}\left(C_{S_{8(s)}} - K_{sp,S_8}\right) + 1{*}10^{-10}k_{S_{8(s)}}\frac{C_{S_{8(l)}}}{\varepsilon_{S_{8(s)}}} \tag{21}$$

As mentioned above, it was considered only $Li_2S_{(s)}$ as unsolvable products derived from polysulfides reduction:

$$R_{Li_2S(s)} = k_{Li_2S_{(s)}}\varepsilon_{Li_2S_{(s)}}\left([C_{Li^+}]^2\left[C_{S^{2-}}\right] - K_{sp,Li_2S}\right) \tag{22}$$

As a result of precipitation and dissolution processes arising from non-Faradaic reactions, the structure of both the cathode and the separator evolve over time. This structural evolution is reflected in changes in porosity, whose time derivative within the domain m can be expressed as:

$$\frac{d\varepsilon_m}{dt} = -\sum V_k R_k \tag{23}$$

Table 2
Kinetic and thermodynamic properties [11].

Reaction (j)	$\mathbf{i_{j,0,ref}}\,[\mathbf{A\ m^{-2}}]$	$\mathbf{E_{j,0,ref}}\,[\mathbf{V}]$
1	2	2.41
2	5e-2	2.35
3	5e-2	2.23
4	2e-4	2.03
5	2e-6	2.01
6	0.5	0

2.5. Modeling polysulfide shuttling

Shuttling can be summarized as a degradation process based on the diffusion of polysulfides towards the anode, the dissolved species can be then gradually reduced until the last oxidation state. At this point, or they can precipitate on the anode surface, leading to a degradation of the interphase or diffusing back towards the cathode, decreasing the coulombic efficiency. During charge, the Li-metal anode acts as a sink point, forming an unfavorable concentration gradient, which contributes to the Fick diffusion of the polysulfides. At the same time, the migration contribution, which is related to the electrolyte potential, acts in the opposite direction, generating a driving force towards the cathode. Experimentally, shuttling is observed as an irreversible capacity decay coupled with a deviation from ideal coulombic efficiency. The model framework was developed trying to provide a qualitative description of shuttling, aiming to a monotonic irreversible capacity decay and a reduction of the coulombic efficiency dependent on time. Therefore, shuttling was described as a chemical reaction using the same scheme to model the electrochemical activity of polysulfides and Li-metal. The reaction rate for shuttling is assumed to be proportional to a time constant k_s, which for the model was chosen arbitrarily, and the concentration of polysulfide at the anode-electrolyte interface, C_{S_i}. The equations set up is reported below.

$$R_{s,i} = k_S\left[C_{S_i}\right](1-\theta)\mathrm{e}^{-\theta} \tag{24}$$

The variable θ is a dimensionless variable, which expresses the irreversible $Li_2S_{(s)}$ precipitated on the Li-metal surface. As polysulfides are consumed at the anode/electrolyte interface, an unsolvable and non-electrochemical active layer is deposited on the surface, limiting further reduction. The purpose of implementing such formulation to describe shuttling is to describe a non-linear, monotonic decrease in capacity followed by stabilization. Each chemical reaction acts as both sink and source for the individual polysulfides until the last reduction state, S^{2-}, which precipitation on the surface was assumed irreversible, following a similar approach employed by K. Yoo et al. [17]:

$$R_{Li_2S_{(l)}} = k_{Li_2S_{(s)}}\left([C_{Li^+}]^2\left[C_{S^{2-}}\right]\right) \tag{25}$$

$$\frac{d\theta}{dt} = \frac{R_{Li_2S_{(l)}}}{1[molm^{-3}]} \tag{26}$$

where l is referring to the lost $Li_2S_{(s)}$, precipitated at the anode surface, and considered as irreversibly lost.

2.6. Boundary conditions

2.6.1. Cathode/current collector interface

The cathode current collector stands as physical barrier for the diffusion of the dissolved species, therefore the flux of each species i must be set equal to zero at this point:

$$N_i|_{x=l_{sep}+l_{pos}} = 0 \tag{27}$$

Furthermore, the current at the interface is imposed equal to the external current density applied and it's carried out only by the solid phase, therefore the liquid-phase current is equal to zero:

$$i_s|_{x=l_{sep}+l_{pos}} = I_{app} \tag{28}$$

$$i_l|_{x=l_{sep}+l_{pos}} = 0 \tag{29}$$

2.6.2. Separator/cathode interface

Concerning the mass transport side of the model, at the interface between the separator and the cathode, the continuity of the flux for each species dissolved inside the electrolyte has to be guaranteed:

Table 3
Precipitation kinetics parameters [8,11].

Precipitate (k)	Rate constant(k_k)	Solubility product ($k_{sp,k}$)	Molar volume V_k $\left[m^3mol^{-1}\right]$
$S_{8(s)}$	$5[s^{-1}]$	$19[molm^{-3}]$	256.56
$Li_2S_{(s)}$	1e-4$\left[m^6mol^2s^{-1}\right]$	1e5$[mol^3m^{-9}]$	45.95

$$N_{i,sep}|_{x=l_{sep}} = N_{i,cat}|_{x=l_{sep}} \quad (27)$$

Meanwhile, the current at the interface is carried out by the liquid phase and, as it was done for the flux, has to be set the continuity between each domain. Therefore, the solid current is imposed equal to zero:

$$i_{l,sep}|_{x=l_{sep}} = i_{l,cat}|_{x=l_{sep}} \quad (28)$$

$$i_{s}|_{x=l_{sep}} = 0 \quad (29)$$

2.6.3. Anode/separator interface

The only active species at the anode/separator interfaces are Li^+ ions derived from the electrochemical reduction and oxidation from lithium metal chip. Therefore, for all the dissolved species, except Li^+, the flux is set equal to zero. The liquid phase current is related only to Li^+ flux, meanwhile the solid potential is set to zero:

$$N_{i}|_{x=0} = 0 \quad (30)$$

$$N_{Li^+}|_{x=0} = \frac{i_{Li^+}}{F} \quad (31)$$

$$i_{l}|_{x=0} = FN \quad (32)$$

$$\varphi_s = 0 \quad (33)$$

3. Results and discussion

The purpose of this study is to understand the potential effect of Li^+ diffusivity on the performance of Li—S battery, going from single discharge to galvanostatic cycling. Therefore, four arbitrary scenarios for D_{Li^+} were chosen, all reported in Table 4. The study comprehends a wide characterization for different set-up and parametric conditions to verify the ability of the model to capture the complex behavior of Li—S batteries. Focusing on how polysulfides mass transport and its effects are correlated with Li^+ diffusion kinetic. The selection of the lithium diffusion coefficients D_{Li^+} investigated in this work is based on the wide range of values reported in the literature, obtained from both experimental measurements, such as cyclic voltammetry, electrochemical impedance spectroscopy, and GITT, and from previously developed modeling studies [11,12,22–24].

The model was developed based on a Li-ion cell CR2032 with a theoretical capacity of 2.01[mAh], which corresponds to a mass of active sulfur of 1.2[mg], assuming as counter electrode a lithium metal foil and as separator Celgard 2500. All the parameters used for cell geometry and structure are reported in Table 5.

Table 4
Li^+ diffusivity case study [11,12,22–24].

Scenario	D_{Li^+} $\left[m^2s^{-1}\right]$
1^{st}	0.88e − 10
2^{nd}	0.88e − 11
3^{rd}	0.88e − 12
4^{th}	0.44e − 12

Table 5
Geometrical parameters [11].

Parameter	Value
l_{sep}	25e − 6 $[m]$
l_{pos}	20e − 6 $[m]$
A	1.76e-4 $[m^2]$
a_v	1e5 $[m^{-1}]$
$\varepsilon_{S_8,sep}$	1e − 7 [−]
$\varepsilon_{S_8,cat}$	0.14 [−]
$\varepsilon_{Li_2S,sep}$	1e − 7 [−]
$\varepsilon_{Li_2S,cat}$	1e − 7 [−]
$\varepsilon_{0,sep}$	0.55 [−]
$\varepsilon_{0,cat}$	0.7 [−]
σ	1 $[Sm^{-1}]$
ξ	1.5

3.1. Li^+ diffusivity as source of reversible losses

In lithium-sulfur batteries, capacity fading arises from a combination of reversible and irreversible processes. Reversible losses are typically associated with the dissolution of lithium polysulfides, and all that comes within a conversion system, where the active species can be easily dissolved and move within the electrolyte. Polysulfides can move freely between the porous electrode and the separator, therefore they cannot be easily confined inside the cathode as they are constantly shifted by concentration gradient and electrolyte potential. Leading to marginalized residual material inside non electrochemical active region. Although the intensity of these reversible losses, as the material can still be recovered in future cycle, can change significantly depending on the properties of the system and the condition at which is subjected. Therefore, here is conducted a sensitivity analysis on the effect of Li^+ diffusivity on reversible losses, accounting both for voltage and specific capacity.

The presence of active dissolved materials that can migrate freely inside the electrolyte is what causes shuttling. In essence, shuttling causes irreversible active material losses coupled with the degradation of the anode/electrolyte interphase, leading to both capacity decay and polarization losses. However, as pointed out by Zhang in his paper on reversible losses in Li—S batteries [11]. The mass transport process involving the diffusion of polysulfides is not only responsible for irreversible capacity losses, but also for a limited sulfur utilization, especially at high current intensity [10,25,26]. Zhang proved that the major kinetic limitations with Li—S batteries are not purely related to electrochemical activity but rather dependent on the mass transport of the dissolved species. In the ideal case, polysulfides should be trapped within the porous cathode domain without the possibility to diffuse towards anode. However, in a real case polysulfides are constantly shifted between the cathode and separator, and their distribution is dependent on concentration gradient and migration. During discharge, polysulfides are produced inside the cathode due to the electrochemical reduction of sulfur, creating a concentration gradient that is unbalanced with respect to the separator, allowing their diffusion according to Fick's law. However, this imbalance is not persistent during discharge and changes depending on the state of discharge (SOD). In parallel, a second contribution to mass transport is generated by electrolyte potential, in particular the potential gradient within the electrolyte. As the polysulfides are negatively charged species, they lean towards higher potential, and this behavior is responsible for migration contribution in the

Nernst-Planck equation.

Galvanostatic discharge was modelled, at different constant current, going from to 0.1C, 0.5C and 1C with a cut-off voltage of 1.8[V], to provide a wider understanding on how a limited lithium diffusivity can play a role on sulfur utilization. All the four-case scenario for Li^+ diffusivity were taken in consideration to understand how the several order magnitudes can actually influence the final performance at different current intensities. Hence in Fig. 1a,c and e are reported the comparison of the voltage profile vs. specific capacity at 0.1C,0.5C and 1C, which correspond respectively to a current density of 1.192, 5.96 and 11.92[Acm^{-2}]. Firstly, the model is able to reproduce the typical discharge behavior of a Li—S battery, regardless of the current intensity applied, consisting of two distinct plateau and a supersaturation point in between, label for clearness, with the first voltage plateau associated to the reduction of long chain polysulfides and the second with intermediate and short. In the case of low applied current, as shown in Fig. 1a corresponding to a rate of 0.1C, the effect of lithium diffusivity on the discharge profiles is marginal. The delivered capacities nearly matched each other, with no remarkable differences observed along the discharge, except for a more pronounced polarization in the case of lower lithium diffusivity in the second plateau. For a more comprehensive analysis, the distribution of the electric potential of the electrolyte within the separator is also reported in Fig. 1b, d, and f. As can be observed the lower lithium diffusivity of lithium leads to a more pronounced electrolyte polarization, which consequently affects the migration term in the mass transport equations. At intermediate C-rates, such as 0.5C, differences in both the discharge profiles and the delivered capacity can be noticed. While cases 1st and 2nd, characterized by higher diffusivity, still show an overlapping profile, a reduction in lithium diffusivity by one order of magnitude results in a capacity loss of

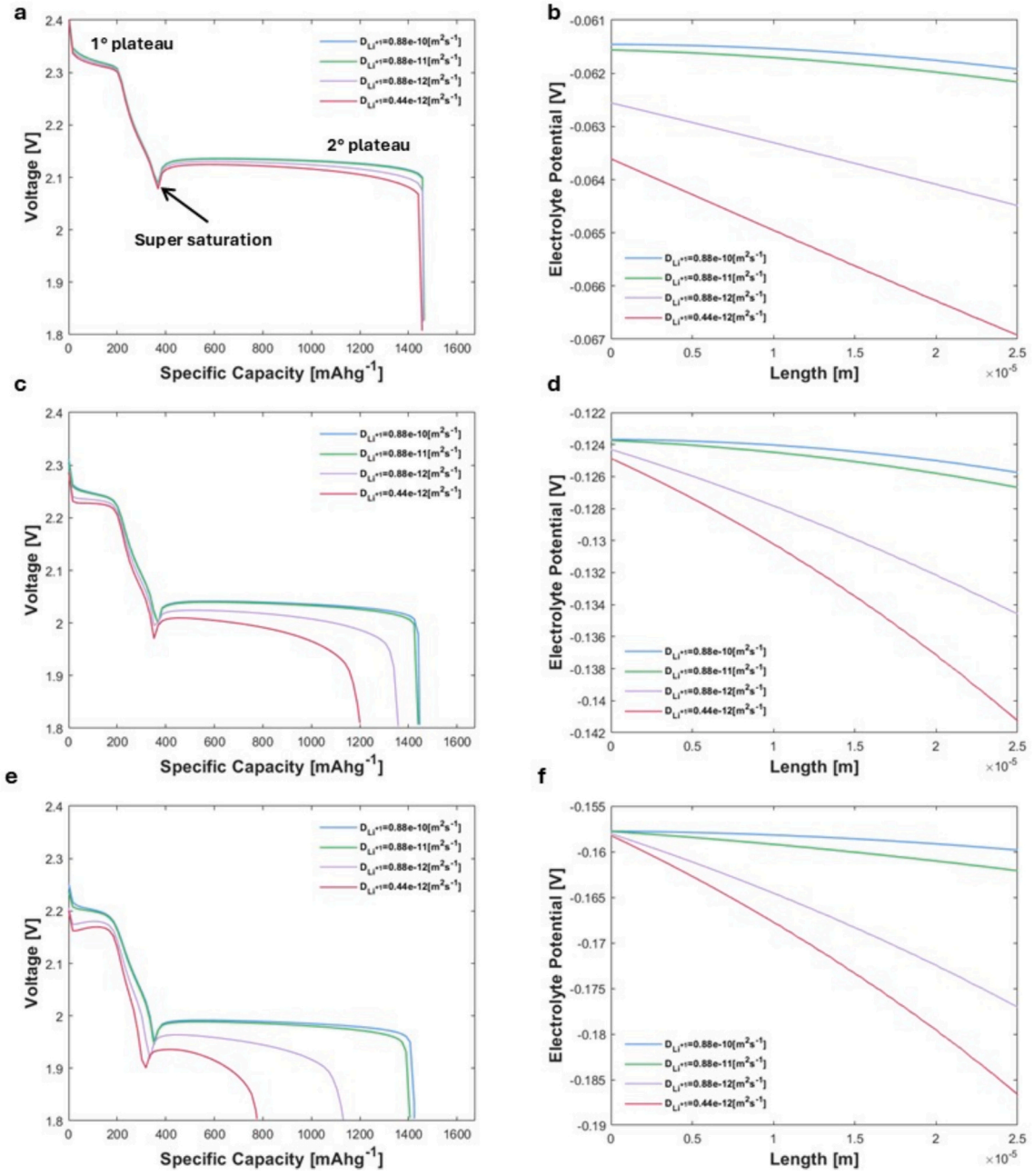

Fig. 1. Understanding the effect D_{Li^+} on reversible capacity losses at different current intensity: a,c,e) Voltage profile vs Specific Capacity respectively at 0.1,0.5 and 1C. b,d,f) Electrolyte potential profile vs length inside the separator at 25% SOD[%] respectively at 0.1,0.5 and 1C.

approximately 100[mAhg^{-1}], meanwhile for the lowest diffusivity case, this reduction exceeds 200[mAhg^{-1}]. This capacity loss primarily affects the second plateau, thus involving intermediate and short chain polysulfides, while a strong electrolyte polarization induced by the higher applied current is still observed, leading to higher potential losses. In contrast, during the first plateau, the main difference is associated with a voltage drop that causes a noticeable shift in the dissolution of solid sulfur and the subsequent formation of long-chain polysulfides. At higher current rates, such as 1C, Fig. 1e and f, the role of lithium diffusivity becomes dominant in determining sulfur utilization. In these conditions, the delivered capacity is nearly reduced by half compared to cases with more favorable transport properties, with the reduction affecting both discharge plateaus. This behavior is further analysed in Fig. 2, where the evolution of intermediate polysulfide species (S_4^{2-}) is reported for both the cathode and the separator. A slower Li^+ diffusivity therefore corresponds to a reduction of sulfur utilization, leading to a limited capacity, introducing the so-called reversible losses.

The reason behind the reduction of the delivered capacity is related to the inhomogeneous distribution of active dissolved species within the computational domain. In Fig. 2 is reported the evolution vs. SOD[%] of the average concentration[molm^{-3}] of S_4^{2-} inside the cathode and the separator [11,24]. It was chosen S_4^{2-} as it is an intermediate polysulfide present during both the first and second plateau. Fig. 2a, c, and e, corresponding to current rates of 0.1C, 0.5C, and 1C, respectively, report the evolution of species concentrations within the cathode during discharge for all the four cases under investigation. Consistently with the discharge profiles, lithium diffusivity does not play a significant role at low current rates. Indeed, the concentration profiles largely overlap. The

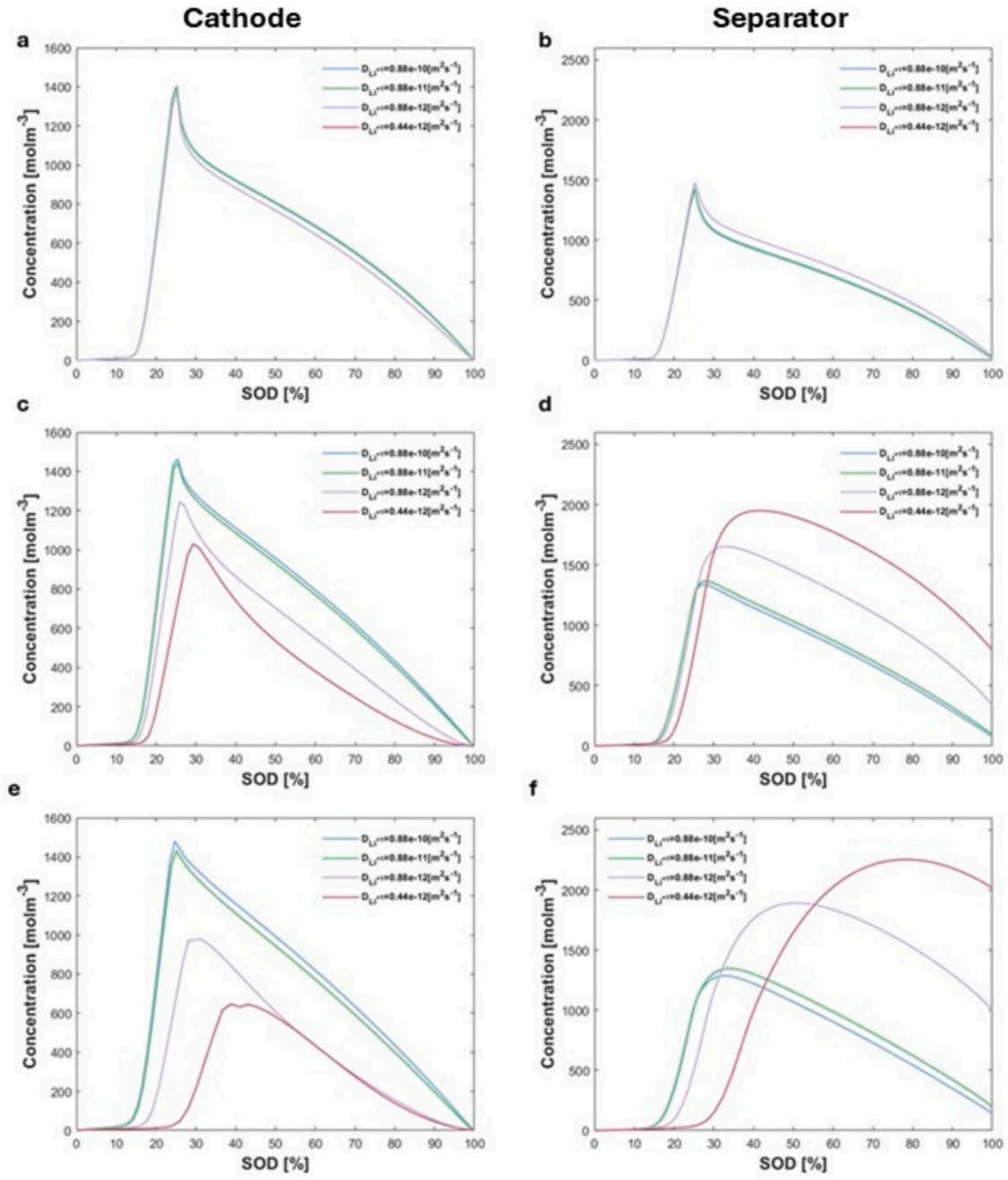

Fig. 2. Understanding the effect D_{Li^+} on reversible capacity losses at different current intensity a,c,e) Average S_4^{2-}concentration inside the cathode vs SOD respectively at 0.1,0.5 and 1C. b,d,e) Average S_4^{2-} concentration inside the separator vs SOD respectively at 0.1,0.5 and 1C.

higher sulfur utilization at low currents, corresponding to an increased specific capacity, is correlated by a negligible residual amount of polysulfides inside the separator at the end of discharge. During discharge, the combined effect of concentration gradients and electrolyte potential gradients governs the mass transport behavior of dissolved polysulfides [11]. Due to their negative charge, polysulfides tend to migrate towards regions of higher electric potential leading to their accumulation within the separator. As for system with lower Li^+ diffusivity, in order to maintain the overall electroneutrality of the electrolyte, polysulfides migrate to compensate for the localized accumulation of lithium ions. Subsequently during discharge, the concentration gradient reverses, driving polysulfides back towards the cathode, by Fick diffusion, to complete their electrochemical reduction. As the applied current increases, the reduction in delivered capacity can be directly correlated with the corresponding concentration profiles. The effect of lithium diffusivity leads to both a progressive decrease in concentration levels and a shift towards higher states of discharge. This behavior will be further discussed in Fig. 3, where the evolution of solid-phase fractions are analysed as a function of current intensity and lithium diffusivity. A crucial observation is the increasing amount of intermediate chain polysulfides remaining inside the separator at the end of discharge as the current rises. Although this polysulfides are not irreversibly lost and remain, in principle, electrochemically active, they could not be exploited due to kinetic limitations associated with reduced lithium diffusivity. In particular, at 1C, Fig. 2f, the residual polysulfides concentration in the lowest diffusivity case is approximately four times higher than in kinetically favorable conditions, leading to what can be described as reversible capacity losses.

The model framework also allows us to investigate how the Li^+ diffusivity can impact on the dissolution of $S_{8(s)}$ and the precipitation of

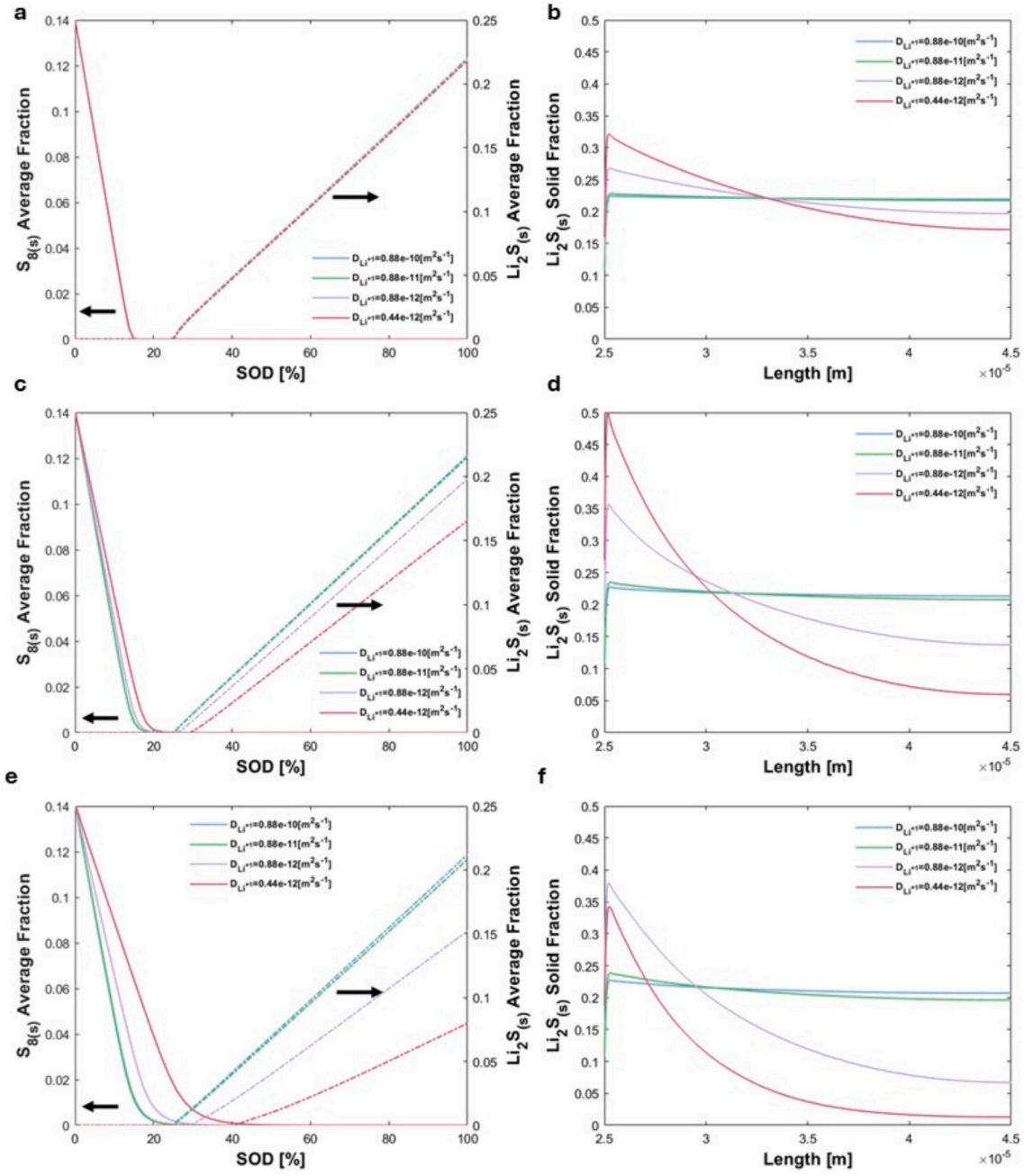

Fig. 3. Understanding the role of D_{Li^+} on non faradaic reaction: a,c,e) Solid fraction profile vs SOD, left y-axis S_8 right y-axis Li_2S, respectively at 0.1,0.5 and 1C. b,d, f) $Li_2S_{(s)}$ distribution vs length inside the cathode at the end of discharge respectively at 01,0.5 and 1C.

$Li_2S_{(s)}$. Indeed, as severally reported in literature through modeling studies [10,27,28], the performance of Li—S batteries are dependent also on non-faradaic reactions, which have a distinct kinetic in comparison to the electrochemical activity of dissolving polysulfides. $Li_2S_{(s)}$ has been discussed to play a critical role on both short- and long-term performance. Facilitating the precipitation of S^{2-} polysulfides within the cathode domain could be beneficial not only to exploit more sulfur but also to limit the concentration inside the electrode, reducing the losses for shuttling and also reducing potential losses [13,26,29,30]. In agreement with the results previously reported in Figs. 1 and 2, at low current densities the effect of lithium diffusivity is marginal on the deposition and dissolution kinetics. Under these conditions, the profiles nearly overlap, indicating a negligible role played by transport limitations. As the current density increases, the dissolution reaction of sulfur with respect to the state of discharge becomes progressively slower, leading to a shift in the complete dissolution to values beyond 20% of SOD, becoming more relevant as the diffusivity on Li^+ is hindered, justifying the shift in concentration reported in Fig. 2. Moreover, despite a comparable average solid fraction of $Li_2S_{(s)}$ deposited within the cathode structure, Fig. 3b shows that, when moving towards systems characterized by lower lithium diffusivity, therefore limiting the possible amount of available Li^+ within the cathode, a less homogeneous distribution of the precipitate within the cathode matrix is observed, and this become more remarked as the current rate increases Fig. 3d and f. A similar behavior was reported by Ghaznavi and Chen in their study on the rate constant for $Li_2S_{(s)}$ [12]. Their model predicted that the porous cathode leans towards a more uniform structure at the end of discharge when the set-up shifts towards faster kinetics. Thus process is typical of conversion system such as Li—S batteries where electrochemical process and faradaic reaction are interconnected, and so are involved phenomena with different kinetic [12,26]. However, a more pronounced effect is observed on $Li_2S_{(s)}$ deposition with an increase of the current intensity. Where, by moving towards higher current and system with lower Li^+ diffusivity, there is compressive reduction of the total amount of $Li_2S_{(s)}$ precipitated within the cathode structure. A reduction of the precipitate leads to an increased accumulation of short chain polysulfides. As terminal reaction products, these species induce a shift in the equilibrium potentials, resulting in enhanced polarization of the system, as evidenced by the discharge profiles in Fig. 1. For the system with lowest diffusivity, the evolution of the distribution and peak intensities is clearly non-linear. At 0.1C, the system exhibits overall homogeneous deposition with a relatively higher amount of precipitate closer to the cathode-separator interphase. At 0.5C, although the total deposited amount decreases, more localized and intense peaks emerge. Finally, at 1C, the peak intensity becomes comparable to the 0.1C case, but with markedly stronger spatial inhomogeneities. These phenomena also impact the morphological properties of the cathode. Indeed, the deposition process is accompanied by a reduction in porosity, which in turn deteriorates transport kinetics. Consequently, the relationship between diffusion and these processes is not simply proportional. For completeness, the evolution of the effective diffusion coefficient, corrected according to Eq. (12), is reported in the Supporting Information.

3.2. Shuttle implementation in the model and sensitivity analysis

Before starting to investigate the effect of Li^+ diffusivity on long cycle performance, it is important to verify that the framework used is able to capture the major effect of shuttling: a) a monotonic source of irreversible capacity losses and b) reduction of coulombic efficiency. Shuttling is a time dependent process, increasing the charging or enhancing the reaction time provides more time to the polysulfides to diffuse towards the anode and so facilitating the irreversible capacity decay. Similarly, by enhancing the degradation reaction, for a given time the corresponding effect on the voltage profile will be amplified [6,16,17]. To verify the accuracy of the model, in Fig. 4a a parameter analysis, performed by discharging and charging the cell with the same current intensity of 0.1C, is reported. The purpose is to investigate the effect of the shuttling constant k_s during charge, expecting a gradual increase of the charging time with constant use. As expected, the capacity needed to fully recharge the cell increases with k_s, until the theoretical threshold is exceeded. However, interestingly a non-linear behavior is present. As mentioned above, during charge the migration field drives the polysulfides towards the cathode to be recovered, meanwhile the anode acts as sink. As the kinetic constant increases, the polysulfides losses are enhanced, strengthening the concentration unbalancing, and so limiting the migration effect.

Furthermore, the cell was galvanostatic discharged until the voltage cut-off of 1.8[V] at a constant current of 0.1C to be then immediately charged without any rest time in between until a voltage cut-off of 2.6 [V] was reached at four different current intensity to investigate the rate dependency of shuttling. A wide range of charging current density was chosen to verify the capability of the model to capture the effect of charging time. In summary, were used current density J of 0.358,0.596,1.192 and 2.384[Am^{-2}] were used, corresponding respectively to a current rate of 0.03,0.05,0.1 and 0.2C. During charge, the first noticeable difference is the shift of the plateau as the current increases, leading to a gradual increase of the voltage and a visual overpolarization. The model used a dilute description for the electrolyte properties, therefore the plateau shift can be justified to an increase of the activation current, and so electrochemical limitations. The charging

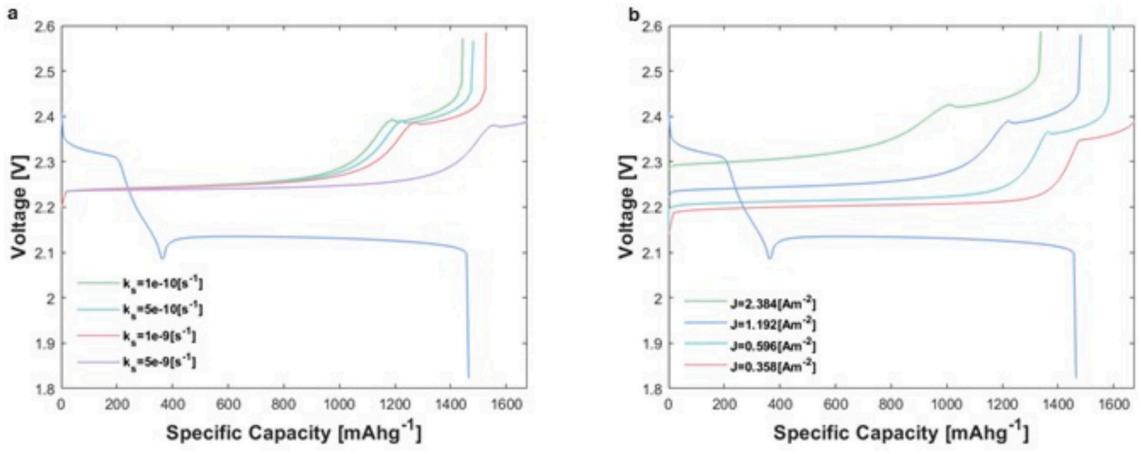

Fig. 4. Parameter analysis on shuttling, using 2nd case of D_{Li^+}: a) Charge and discharge Voltage profile vs specific capacity at 0.1C with different shuttle constant $k_s[s^{-1}]$ b) Charge and discharge Voltage profile vs specific capacity at different current intensity, using k_s = 1e-9[s^{-1}].

plateau starts to gradually stretch as the current intensity decreases, until at 0.03C, which corresponds to a current density J of 0.358[Am^{-2}], the specific capacity needed exceeds the theoretical one. In the approach followed, shuttling is described as a chemical reaction with a defined kinetic constant. By decreasing the charging current, the diffusion of polysulfides, which is a significantly slower process in comparison to electrochemical activity is facilitated. Allowing higher concentration towards the anode, corresponding to higher losses and limited coulombic efficiency.

In parallel with single charge-discharge studies performed over an individual cycle; the setup was used under continuous cycling in order to assess the model sensitivity over a larger number of cycles. Specifically, galvanostatic cycling was carried out without rest periods at a current rate of 0.05C, corresponding to a current density J of 0.596[Am^{-2}], for a total of 15 cycles. This operating current was chosen to match the time dependent scale of shuttling. As shown in Fig. 5a, in the case of low reaction kinetic constants, even at very low current intensities, conditions that would typically enhance the shuttling effect, the resulting capacity retention profiles remain relatively flat. This behavior arises from, as discussed in the previous section, reversible losses become significant at higher current intensities. However, in the range of a shuttling constant k_s between $10^{-10}$and 10^{-9}, more pronounced differences begin to emerge, also coupled with the evolution of the coulombic efficiency. In particular, for the case study with a kinetic constant of 5×10^{-9}, a substantial capacity loss is already evident from the first cycle. This loss remains significant but gradually decreases over subsequent cycles. This trend reflects a progressive reduction of the active lithium surface area available for further reactions. This interpretation is further supported by the evolution of the parameter θ, as reported in Fig. 5c, where the marked differences in orders of magnitude are consistent with the predicted trends in both capacity retention and coulombic efficiency.

Overall, the framework used provides a valid and accurate description of shuttling, in accordance with the available literature, being able to capture its dependence on the charging time and its role on limiting the coulombic efficiency.

3.3. Long cycle studies on Li^+ diffusivity and irreversible capacity losses

The model was constantly galvanostatic charged and discharged at a constant current of 0.05C to investigate the role of Li^+ diffusivity on the irreversible decay generated by shuttling. As explained above, given the time dependency of shuttling, it was chosen a small current to reduce the contribution of reversible capacity losses [11]. In Fig. 6a is reported the comparison for the specific capacity evolution vs the number of cycles between all the cases under analysis, coupled also with the coulombic efficiency. Meanwhile, in Fig. 6b is also reported the evolution of the factor θ to describe the gradual degradation of the anode-electrolyte interphase and provide a more accurate look on the irreversible losses. It is also reported for a better understanding that the comparison between charge and discharge capacity for each single case under study, and also in Table 6 are reported the initial and final values, coupled also with the absolute and relative losses.

The diffusivity of Li^+ does not play a significant role in the capacity delivered at small current intensity, as discussed above, indeed the difference at the beginning is minimal, with all the four cases almost overlapping. The kinetic mismatch between diffusion and electrochemical activity is enhanced at higher currents, leading to the introduction of so-called reversible losses. Vice versa, at lower current

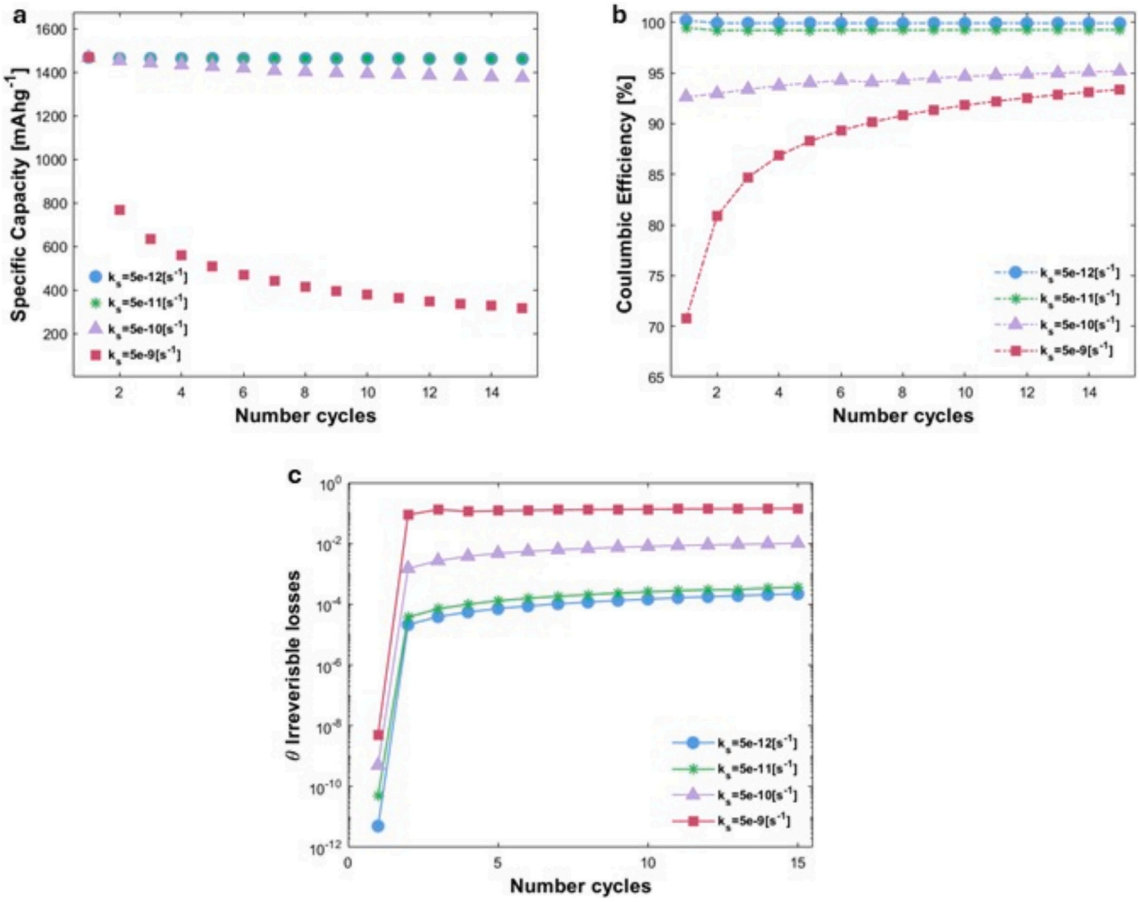

Fig. 5. Sensitivity analysis on the role of shuttling constant, k_s, using 2nd case of D_{Li^+}, using a current rate of 0.05C: a) Specific capacity vs number cycles b) Coulumbic efficiency vs number c) θ irreversible losses vs number cycles, y-axis in log scale.

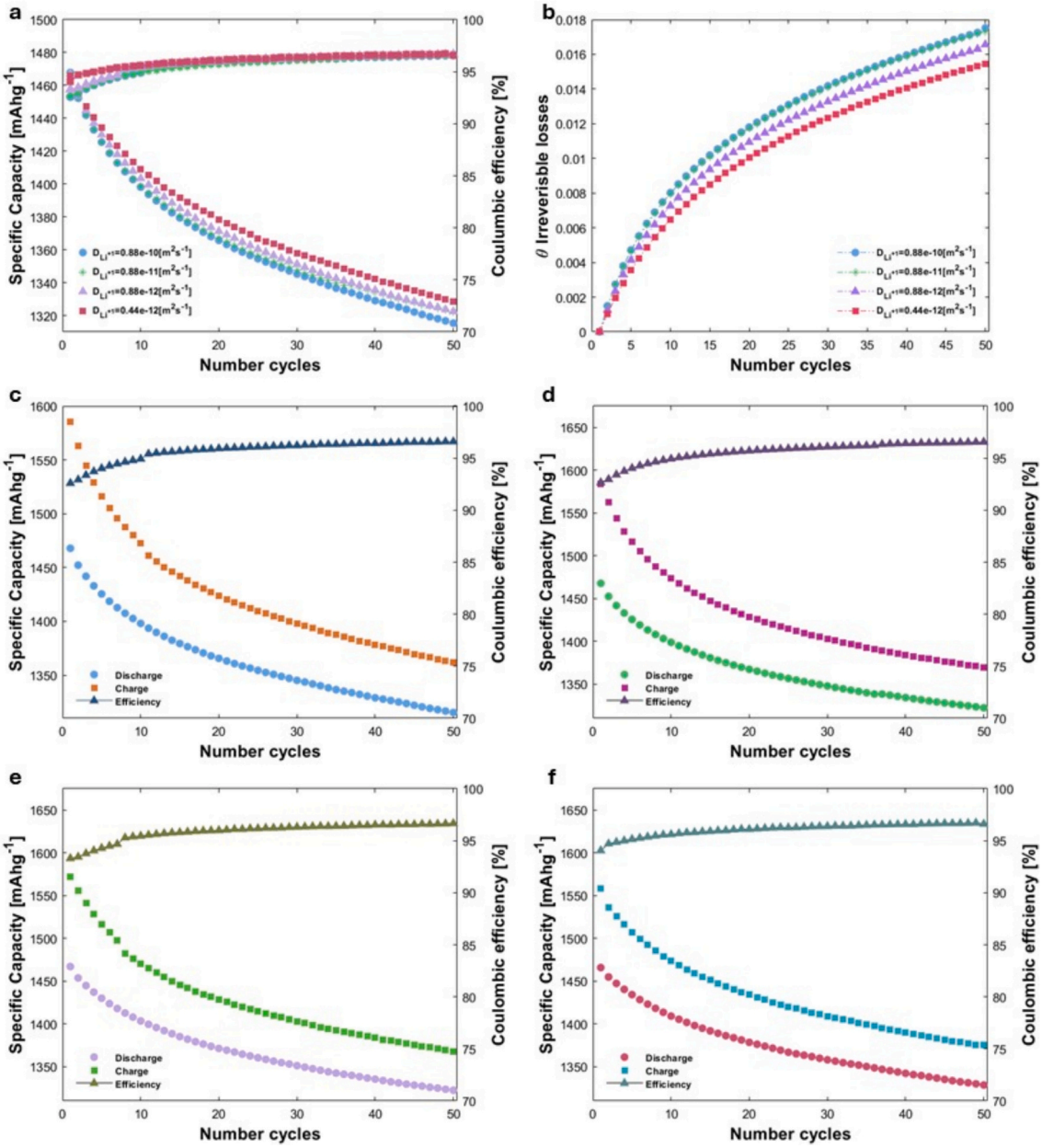

Fig. 6. Comparison specific capacity evolution using k_s = 1e-9[s^{-1}] at constant current rate of 0.05 a) Discharge specific capacity and coulombic efficiency vs number of cycles b) θ irreversible losses vs number cycles, y-axis in log scale c) Discharge, Charge and coulombic efficiency vs number of cycles 1st case of D_{Li^+} d) Discharge, Charge and coulombic efficiency vs number of cycles 2nd case of D_{Li^+} e) Discharge, Charge and coulombic efficiency vs number of cycles 3rd case of D_{Li^+} f) Discharge, Charge and coulombic efficiency vs number of cycles 4th case of D_{Li^+}.

Table 6
Long cycling comparison.

Case	**1st** cycle [mAhg^{-1}]	**50th** cycle [mAhg^{-1}]	ΔQ [mAhg^{-1}]	ΔQ [%]
1st	1467.9	1315.3	152.6	10.39
2nd	1467.8	1322.3	145.5	9.89
3rd	1467	1322.4	144.6	9.85
4th	1465.8	1328.5	137.3	9.36

intensity the polysulfide has more time to diffuse back guaranteeing a higher sulfur utilization. However, the capacity decay becomes more predominant as the diffusivity of Li^+ increases, as was also reported by F. Lama and his colleagues in an experimental study on diffusional features of microporous carbon [22]. Proving that shuttling is not only determined by the time available for the parasitic reaction to occur, but also on the mass transport behavior of the dissolved species. Indeed, similarly to what happens during discharge, the slower Li^+ diffusivity causes stronger potential gradient within the electrolyte, enhancing migration, which facilitates the trapped polysulfides in the separator to diffuse towards the cathode. A slow Li^+ diffusivity reduces irreversible losses and also guarantees a higher coulombic efficiency, as can be observed in Fig. 6b, in systems characterized by high lithium diffusivity, a variation of one order of magnitude does not lead to any significant difference in performance. In contrast, when moving towards lower orders of magnitude, while still remaining within the same diffusivity range, a noticeable difference emerges in the amount of lithium polysulfides irreversibly deposited at the interface. This accumulation directly contributes to the degradation of the lithium metal anode, leading to a progressive reduction of the active charge-transfer interface. As a consequence, increased interfacial resistance arises, ultimately resulting

in more pronounced overpotentials during cell operation. Beyond the work of Lama and co-workers, the role of lithium diffusivity emerges as a crucial factor in the engineering of electrolytes for Li—S batteries. Variations in electrolyte viscosity, in particular, can significantly influence sulfur utilization and overall cell performance. Lower-viscosity configurations generally promote higher lithium diffusivity, which enhances sulfur utilization, especially at high C-rates. Conversely, more viscous electrolytes tend to suppress parasitic phenomena, leading to improved capacity retention. Indeed, dedicated studies on electrolyte systems with varying concentrations of LiTFSI salt have shown that low-concentration electrolytes, characterized by higher lithium diffusivity, are associated with improved sulfur utilization, particularly under high current conditions. On the other hand, increasing the salt concentration results in more viscous electrolytes, where the primary benefit lies in enhanced capacity retention. This improvement is mainly attributed to the mitigation of the shuttling effect, as reduced the mobility of Li^+ affecting consequently the migration of soluble polysulfides [21,25,31,32].

These findings highlight the intrinsic trade-off between transport properties and electrochemical stability: while high diffusivity favours reaction kinetics and active material utilization, increased viscosity contributes to the stabilization of the system by reducing detrimental side reactions.

Fig. 7 shows the concentration of S_4^{2-} at the anode electrolyte interphase during both charge and discharge for the 1st,30th and 50th cycle for each case scenario. During discharge, as discussed in detail in the previous section, polysulfides are pushed by migration far from the cathode in order to compensate for the accumulation of Li^+ at the anode-electrolyte interphase, and so guarantee the charge neutrality of the system. This generates a favorable condition for the accumulation of dissolved polysulfides at the Li-metal anode, causing a difference in the capacity delivered, as reported in Table 6. Therefore, even at small current intensity, the Li^+ diffusivity plays a role in the mass transport behavior of polysulfides. Meanwhile, the migration contribution facilitates during charge the prevention from shuttling, limiting their concentration near the anode, despite a less favorable condition in discharge. Reducing shuttling and so guaranteeing at the end a higher capacity retention. However, as the number of cycles increases the difference gradually becomes less remarkable, especially during charge. As shown in Fig. 6, the capacity decay is not purely linear, indeed the specific capacity shows almost a plateau as the number of cycle increases. Justifying a mitigation of shuttling effect on the transport process of polysulfides.

Lastly, in Fig. 8 is reported for each case scenario the voltage vs specific capacity profile for the 1st,30th and 50th cycle for each case study, which overall show a similar behavior. Regardless of the cycle, all the profiles match the one expected from a Li—S batteries, showing two distinct plateau and a supersaturation point which decreases intensity with the number of cycles. Furthermore, it can be noticed a significant over polarization during both charge and discharge, increasing the overall voltage hysteresis. Those model predictions are in agreement with experimental and modeling studies on shuttling, also reported inside the supporting information, which predicted or reported an overall over polarization with the number of cycles [16,22]. The over polarization of the voltage profile follows a similar trend with the capacity decay, getting less predominant with the number of cycles. As the number of cycles increases, the number of available materials for electrochemical activity is reduced, leading to higher activation losses. As can be seen, both first and second plateaus are affected by the reduction of the capacity delivered, which as shown before becomes less predominant over cycling.

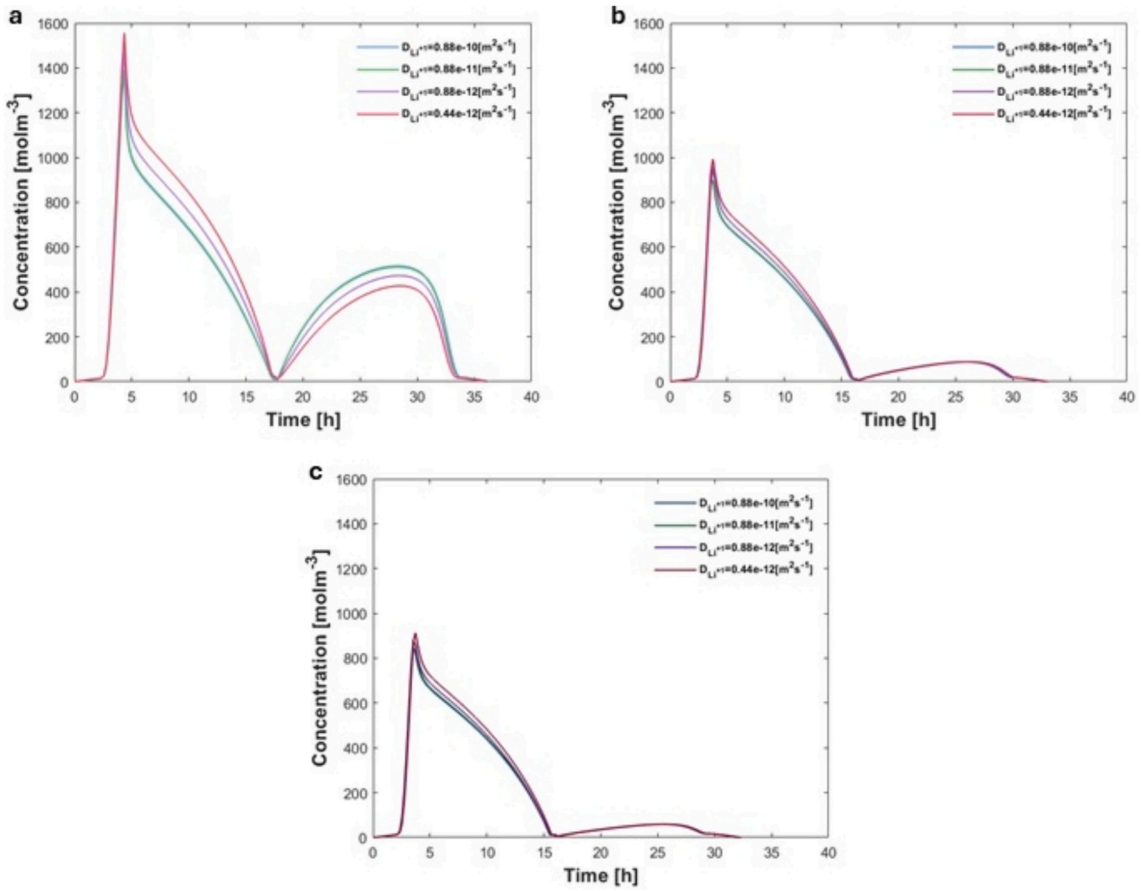

Fig. 7. Comparison point concentration at the anode electrolyte interphase for S_4^{2-} using k_s = 1e-9[s^{-1}] a) 1st cycle b) 30th Cycle c) 50th Cycle.

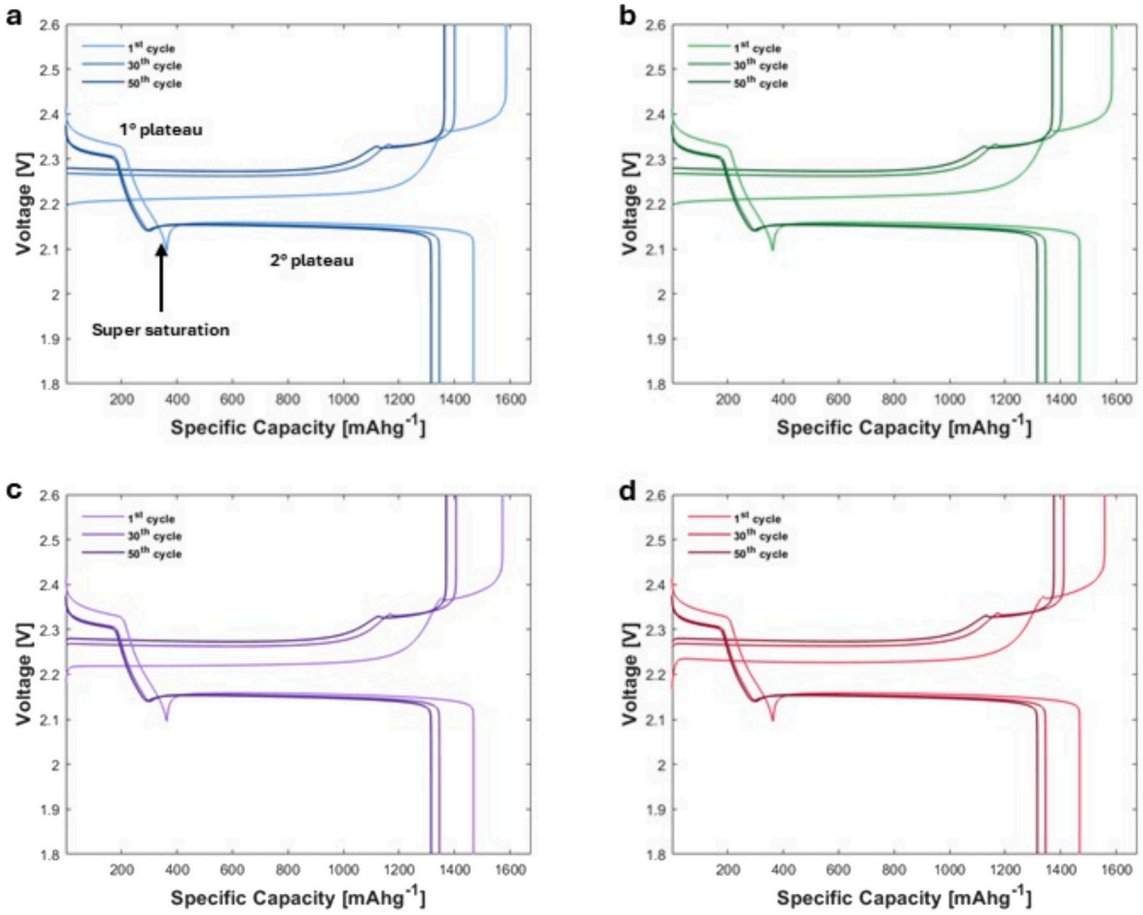

Fig. 8. Comparison charge and discharge voltage profile vs specific capacity for the 1st,30th and 50th cycle using $k_s = 1e\text{-}9[s^{-1}]$ a) 1st case D_{Li}^{+} b) 2nd case D_{Li}^{+} c) 3rd case D_{Li}^{+} d) 4th case.

4. Conclusion

The results here discussed proved the ability of the modeling framework to supply a wide perspective on the mass transport behavior of the dissolved species present in Lithium-Sulfur batteries, extending the study for several numbers of cycles in a 1D domain. The model has been used to perform a wide parametric analysis on the role of Li^+ diffusivity on the transport behavior of polysulfides and its consequences on both reversible and irreversible capacity losses, highlighting also its effect as source for potential losses, which are crucial in a system with such short voltage window. The model's results show that at even relative low current intensity, such as 0.5C, a significant reduction of the capacity delivered is observable by reducing the diffusivity of Li^+, which is not dependent on irreversible process but only on the limited diffusion of dissolved polysulfides due to the electrolyte potential state. Such losses become more predominant as the current rate increases, reducing the capacity delivered by almost half at 1C. Furthermore, the model allowed to investigate the role of Li^+ diffusivity on the structure evolution within the cathode structure, crucial in a conversion system as Li—S batteries, highlighting overall a reduction of the average solid $Li_2S_{(s)}$ deposited and a less homogenous distribution, with following consequence on the mass transport properties of the dissolved species. Proving also the flexibility of the model framework to be used in different conditions and set up properties. In this study was provided a valid approach for the implementation of shuttling in 1D domain, guaranteeing fidelity with experimental studies, capturing the time dependencies of such degradation phenomena and its effect on the coulombic efficiency. The long cycling analysis proved the positive effect of slow Li^+ diffusivity to prevent irreversible capacity losses and increase the coulombic efficiency. The migration contribution of polysulfides prevents their accumulation at the anode/separator interphase, limiting the irreversible losses regardless of the current applied or the available time. Proving that at low current intensity, reducing the diffusivity of Li^+ within the electrolyte can be beneficial to mitigate shuttling without reducing significantly the capacity delivered.

Overall, the framework used for the model has been proved an interesting approach to describe shuttling, showing how there is not a single approach for the future development of Lithium-Sulfur batteries, and how its crucial to look for a trade off between single and long-term results.

CRediT authorship contribution statement

Tommaso Filippo Lupatelli: Writing – review & editing, Writing – original draft, Software, Methodology, Conceptualization, Data curation. **Massimo Santarelli:** Visualization, Supervision, Writing – review & editing. **Silvia Bodoardo:** Supervision, Resources, Funding acquisition, Project administration. **Daniele Versaci:** Visualization, Validation, Conceptualization, Methodology.

Declaration of competing interest

The authors declare that they have no known competing financial interests or personal relationships that could have appeared to influence the work reported in this paper.

Acknowledgements

T.F. Lupatelli acknowledges Stellantis - CRF (Centro Ricerche Fiat) for co-funding the Ph.D. scholarship.

This publication is part of the project PNRR-NGEU which has received funding from the MUR – DM 117/2023.

Appendix A

Table 7
Acronym/parameter list.

Symbol	Physical/value meaning	Reference
C_i	Concentration of the dissolved species i	
$C_{i,ref}$	Reference concentration of the dissolved species i	[11]
$\varepsilon_{0,m}$	Initial porosity of domain m	[11]
r_j	Reaction rate for the electrochemical reaction j	
R_j	Reaction rate for the non-faradaic reaction j	
$D_{i,m,eff}$	Effective diffusive coefficient for the species i	
$D_{i,m,0}$	Diffusive coefficient for the species i	[11,12,22–24]
σ	Cathode electric conductivity	[11]
a_0	Specific initial active area	[11]
Ξ	Corrective coefficient specific active area	[11]
k_{S_8}	Rate constant sulfur dissolution/precipitation	[11]
k_{Li_2S}	Rate constant lithium polysulfide dissolution/precipitation	[8]
K_{sp,S_8}	Solubility product sulfur	[8,11]
K_{sp,Li_2S}	Solubility product lithium polysulfide	[8]
V_{S_8}	Molar volume sulfur	[8,11]
V_{Li_2S}	Molar volume lithium polysulfide	[8,11]
k_s	Shuttle constant	
U_j	Equilibrium potential for the electrochemical reaction j	
$i_{o,ref\,j}$	Reference activation current for the electrochemical reaction j	[11]
n_j	Activation overpotential for the electrochemical reaction j	
θ	Irreversible losses	
F	Faraday constant	
T	Temperature	
R	Gas constant	
$\propto_{c,a}$	Cathodic/anodic electron transfer	[11]
$q_{i,j}$	Butler Volmer anodic transfer coefficient	
$p_{i,j}$	Butler Volmer cathodic transfer coefficient	
N_i	Flux for species i	
z_i	Charge species i	[11]
φ_s	Solid phase potential	
φ_l	Liquid phase potential	

Table 8
Governing equation.

Equation	Number
$\frac{d(\varepsilon_m C_i)}{dt} = -\nabla \bullet N_i + r_i + R_i$	(9)
$r_i = a\sum \frac{s_{i,j} i_j}{n_j F}$	(10)
$N_{i,k} = -D_{i,m,eff}\frac{dC_i}{dx} - \frac{z_i D_{i,m,eff}}{RT} F C_i \frac{d\varphi_l}{dx}$	(11)
$D_{i,m,eff} = D_{i,m,0} * \varepsilon_m^b$	(12)
$i_j = i_{0,ref} * \left\{ \prod_i \left(\frac{C_i}{C_i^{ref}}\right)^{p_{i,j}} exp\left(\frac{\alpha_{a,j} F}{RT} n_j\right) - \prod_i \left(\frac{C_i}{C_i^{ref}}\right)^{q_{i,j}} exp\left(\frac{-\alpha_{c,j} F}{RT} n_j\right) \right\}$	(13)
$n_j = \varphi_s - \varphi_l - U_{j,ref}$	(14)
$U_{j,ref} = U_j^0 - \frac{RT}{n_j F}\sum_i s_{i,j} ln\left[\frac{c_{i,ref}}{1000}\right]$	(15)
$i_l = F\sum_I z_i N_i$	(16)
$i_s = -\sigma \nabla \varphi_s$	(17)
$\nabla i_l = a\sum_j i_j$	(18)
$a = a_o \left(\frac{\varepsilon_{cat}}{\varepsilon_{cat,o}}\right)^{\xi}$	(19)
$\nabla \bullet i_s = \nabla \bullet i_l$	(20)
$R_{S_8(s)} = k_{S_{8(s)}} \varepsilon_{S_{8(s)}} \left(C_{S_{8(s)}} - K_{sp,S_8}\right) + 1 * 10^{-10} k_{S_{8(s)}} \frac{C_{S_{8(l)}}}{\varepsilon_{S_{8(s)}}}$	(21)
$R_{Li_2S(s)} = k_{Li_2S_{(s)}} \varepsilon_{Li_2S_{(s)}} \left([C_{Li^+}]^2 [C_{S^{2-}}] - K_{sp,Li_2S} \right)$	(22)

(*continued on next page*)

Table 8 (*continued*)

Equation	Number
$\frac{d\varepsilon_m}{dt} = -\sum V_k R_k$	(23)
$R_{s,i} = k_S[C_{S_i}](1-\theta)e^{-\theta}$	(24)
$R_{Li_2S_{(l)}} = k_{Li_2S_{(s)}}\left([C_{Li^+}]^2[C_{S^{2-}}]\right)$	(25)
$\frac{d\theta}{dt} = \frac{R_{Li_2S_{(l)}}}{1[molm^{-3}]}$	(26)

Table 9
Boundary conditions.

Equation	Number
$N_{i\|_{x=l_{sep}+l_{pos}}} = 0$	(27)
$i_{s\|_{x=l_{sep}+l_{pos}}} = I_{app}$	(28)
$i_{l\|_{x=l_{sep}+l_{pos}}} = 0$	(29)
$N_{i,sep\|_{x=l_{sep}}} = N_{i,cat\|_{x=l_{sep}}}$	(30)
$i_{l,sep\|_{x=l_{sep}}} = i_{l,cat\|_{x=l_{sep}}}$	(31)
$i_{s\|_{x=l_{sep}}} = 0$	(32)
$N_{i\|_{x=0}} = 0$	(33)
$N_{Li^+\|_{x=0}} = \frac{i_{Li^+}}{F}$	(34)
$i_{l\|_{x=0}} = FN$	(35)
$\varphi_s = 0$	(36)

Appendix B. Supplementary data

Supplementary data to this article can be found online at https://doi.org/10.1016/j.est.2026.122660.

Data availability

No data was used for the research described in the article.

References

[1] Y.-T. Liu, S. Liu, G.-R. Li, X.-P. Gao, Strategy of enhancing the volumetric energy density for lithium–sulfur batteries, Adv. Mater. 33 (2021) 2003955, https://doi.org/10.1002/adma.202003955.

[2] C.D. Parke, L. Teo, D.T. Schwartz, V.R. Subramanian, Progress on continuum modeling of Lithium–sulfur batteries, Sustain. Energy Fuels 5 (2021) 5946–5966, https://doi.org/10.1039/D1SE01090E.

[3] M. Wild, L. O'Neill, T. Zhang, R. Purkayastha, G. Minton, M. Marinescu, G.J. Offer, Lithium sulfur batteries, a mechanistic review, Energy Environ. Sci. 8 (2015) 3477–3494, https://doi.org/10.1039/C5EE01388G.

[4] J. Sun, T. Wang, Y. Gao, Z. Pan, R. Hu, J. Wang, Will lithium-sulfur batteries be the next beyond-lithium ion batteries and even much better? InfoMat 4 (2022) e12359 https://doi.org/10.1002/inf2.12359.

[5] W. Gao, Z. Wang, C. Peng, S. Kang, L. Cui, Accelerating the redox kinetics by catalytic activation of "dead sulfur" in lithium–sulfur batteries, J. Mater. Chem. A 9 (2021) 13442–13458, https://doi.org/10.1039/D1TA00772F.

[6] Y.V. Mikhaylik, J.R. Akridge, Polysulfide shuttle study in the Li/S battery system, J. Electrochem. Soc. 151 (2004) A1969, https://doi.org/10.1149/1.1806394.

[7] M. Marinescu, L. O'Neill, T. Zhang, S. Walus, T. Wilson, G. Offer, Irreversible vs reversible capacity fade of lithium-sulfur batteries during cycling: the effects of precipitation and shuttle, J. Electrochem. Soc. 165 (2018) A6107–A6118, https://doi.org/10.1149/2.0171801jes.

[8] N. Kamyab, P.T. Coman, S.K.M. Reddy, S. Santhanagopalan, R.E. White, Mathematical model for Li-S cell with shuttling-induced capacity loss approximation, J. Electrochem. Soc. 167 (2020) 130532, https://doi.org/10.1149/1945-7111/abbbbf.

[9] K.M. Abraham, J.L. Jiang, A mathematical model for a lithium–sulfur cell, J. Electrochem. Soc. 153 (2006) A1613–A1620, https://doi.org/10.1149/1.2937304.

[10] M. Ghaznavi, P. Chen, Analysis of a mathematical model of lithium-sulfur cells part III: electrochemical reaction kinetics, transport properties and charging, Electrochim. Acta 137 (2014) 575–585, https://doi.org/10.1016/j.electacta.2014.06.033.

[11] T. Zhang, M. Marinescu, S. Walus, G.J. Offer, Modelling transport-limited discharge capacity of lithium-sulfur cells, Electrochim. Acta 219 (2016) 502–508, https://doi.org/10.1016/j.electacta.2016.10.032.

[12] M. Ghaznavi, P. Chen, Sensitivity analysis of a mathematical model of lithium–sulfur cells: Part II: precipitation reaction kinetics and sulfur content, J. Power Sources 257 (2014) 402–411, https://doi.org/10.1016/j.jpowsour.2013.12.145.

[13] T. Zhang, M. Marinescu, L. O'Neill, M. Wild, G. Offer, Modeling the voltage loss mechanisms in lithium–sulfur cells: the importance of electrolyte resistance and precipitation kinetics, Phys. Chem. Chem. Phys. 17 (2015) 22581–22586, https://doi.org/10.1039/C5CP03566J.

[14] M.J. Lacey, Influence of the electrolyte on the internal resistance of lithium−sulfur batteries studied with an intermittent current interruption method, ChemElectroChem 4 (2017) 1997–2003, https://doi.org/10.1002/celc.201700129.

[15] S.D. Talian, J. Moškon, R. Dominko, M. Gaberšček, The pitfalls and opportunities of impedance spectroscopy of lithium sulfur batteries, Adv. Mater. Interfaces 8 (2021) 2101116, https://doi.org/10.1002/admi.202101116.

[16] A.F. Hofmann, D.N. Fronczek, W.G. Bessler, Mechanistic modeling of polysulfide shuttle and capacity loss in lithium–sulfur batteries, J. Power Sources 259 (2014) 300–310, https://doi.org/10.1016/j.jpowsour.2014.02.082.

[17] K. Yoo, M.-K. Song, E.J. Cairns, P. Dutta, Numerical and experimental investigation of performance characteristics of lithium/sulfur cells, Electrochim. Acta 213 (2016) 174–185, https://doi.org/10.1016/j.electacta.2016.07.110.

[18] F. Di Donato, et al., Electrolyte measures to prevent polysulfide shuttle in Lithium–sulfur batteries, Batteries Supercaps 5 (2022) e202200097, https://doi.org/10.1002/batt.202200097.

[19] T. Danner, A. Latz, On the influence of nucleation and growth of S8 and Li2S in lithium-sulfur batteries, Electrochim. Acta 322 (2019) 134719, https://doi.org/10.1016/j.electacta.2019.134719.

[20] T. Danner, G. Zhu, A.F. Hofmann, A. Latz, Modeling of nano-structured cathodes for improved lithium-sulfur batteries, Electrochim. Acta 184 (2015) 124–133, https://doi.org/10.1016/j.electacta.2015.09.143.

[21] Y. Liu, Y. Elias, J. Meng, D. Aurbach, R. Zou, D. Xia, Q. Pang, Electrolyte solutions design for lithium-sulfur batteries, Joule 5 (2021) 2323–2364, https://doi.org/10.1016/j.joule.2021.06.009.

[22] S. Lama, et al., Diffusional features of a Lithium–sulfur battery exploiting highly microporous activated carbon, ChemSusChem 16 (2023) e202202095, https://doi.org/10.1002/cssc.202202095.

[23] C. Park, M. Kanduč, R. Chudoba, A. Ronneburg, S. Risse, M. Ballauff, J. Dzubiella, Molecular simulations of electrolyte structure and dynamics in lithium–sulfur battery solvents, J. Power Sources 373 (2018) 70–78, https://doi.org/10.1016/j.jpowsour.2017.10.081.

[24] F. Sultanov, N. Zhumasheva, A. Dangaliyeva, A. Zhaisanova, N. Baikalov, B. Tatykayev, M. Yeleuov, Z. Bakenov, A. Mentbayeva, Enhancing lithium-sulfur battery performance with biomass-derived graphene-like porous carbon and NiO

nanoparticles composites, J. Power Sources 593 (2024) 233959, https://doi.org/10.1016/j.jpowsour.2023.233959.
[25] J.-K. Song, M. Kim, S. Park, Y.-J. Kim, LiTFSI salt concentration effect to digest lithium polysulfides for high-loading sulfur electrodes, J. Energy Chem. 78 (2023) 574–581, https://doi.org/10.1016/j.jechem.2022.11.038.
[26] T.F. Lupatelli, M. Santarelli, S. Bodoardo, D. Versaci, A pseudo one dimensional model to describe the kinetic limitations in lithium–sulfur batteries, J. Electroanal. Chem. 1008 (2026) 119915, https://doi.org/10.1016/j.jelechem.2026.119915.
[27] Y.X. Ren, T.S. Zhao, M. Liu, P. Tan, Y.K. Zeng, Modeling of lithium-sulfur batteries incorporating the effect of Li2S precipitation, J. Power Sources 336 (2016) 115–125, https://doi.org/10.1016/j.jpowsour.2016.10.063.
[28] A.N. Mistry, P.P. Mukherjee, Electrolyte transport evolution dynamics in lithium–sulfur batteries, J. Phys. Chem. C 122 (2018) 18329–18335, https://doi.org/10.1021/acs.jpcc.8b05442.
[29] W. Hua, H. Li, C. Pei, J. Xia, Y. Sun, C. Zhang, W. Lv, Y. Tao, Y. Jiao, B. Zhang, S.-Z. Qiao, Y. Wan, Q.-H. Yang, Selective catalysis remedies polysulfide shuttling in lithium-sulfur batteries, Adv. Mater. 33 (2021) 2101006, https://doi.org/10.1002/adma.202101006.
[30] J. Sun, Y. Liu, L. Liu, J. Bi, S. Wang, Z. Du, H. Du, K. Wang, W. Ai, W. Huang, Interface engineering toward expedited Li2S deposition in lithium–sulfur batteries: a critical review, Adv. Mater. 35 (2023) 2211168, https://doi.org/10.1002/adma.202211168.
[31] F. Wu, F. Chu, G.A. Ferrero, M. Sevilla, A.B. Fuertes, O. Borodin, Y. Yu, G. Yushin, Boosting high-performance in lithium–sulfur batteries via dilute electrolyte, Nano Lett. 20 (2020) 5391–5399, https://doi.org/10.1021/acs.nanolett.0c01778.
[32] F.Y. Fan, M.S. Pan, K.C. Lau, R.S. Assary, W.H. Woodford, L.A. Curtiss, W.C. Carter, Y.-M. Chiang, Solvent effects on polysulfide redox kinetics and ionic conductivity in lithium-sulfur batteries, J. Electrochem. Soc. 163 (2016) A3111, https://doi.org/10.1149/2.1181614jes.